Proceedings of the 7th World Congress on Civil, Structural, and Environmental Engineering (CSEE'22)
~~Lisbon, Portugal~~ Virtual Conference – April 10 – 12, 2022
Paper No. ICGRE 219
DOI: 10.11159/icgre22.219

Stability Modelling of Clay and Silt Slopes to Evaluate the Feasibility of Rheometer Test Results

Gabriel Urquía[1], Juan Villacreses[2], Laura Ibagon[2], Fabricio Yepez[2]
[1]Universidad San Francisco de Quito
Diego de Robles S/N y Pampite, Quito, Ecuador
gnurquiam@estud.usfq.edu.ec[1]; jvillacreses@usfq.edu.ec[2]

Abstract **–** Stability analyses in slopes require mechanical soil properties. Many laboratory procedures had been developed to obtain mechanical parameters: triaxial undrained tests, direct shear tests, and oedometer tests to mention a few. This paper evaluates the feasibility of rheometer tests results to develop a stability model of clay and silt slopes. SEEP/W and SLOPE/W analyses were developed in GeoStudio, modeling drought and rain periods to evaluate the effect of matric suction in shear strength. Results are compared with similar analysis found in the literature, where traditional tests had been applied. The safety factor evolution has been computed during different weather conditions, where the soil strength evolution has been considered. This research revealed that the rheometer tests are feasible to understand the evolution of slopes' stability.

Keywords**:** stability modeling, seepage modeling, safety factor, rheometer test results

1. Introduction

Landslides can occur as a consequence of weather fluctuation on slopes with high permeable materials. The pore water pressure (PWP) raises [1, 2], the soil bulk density increases, and the apparent cohesion decreases during rain, and consequently these effects reduce the factor of safety, and the loading capacity [3]. In tropical countries such as Ecuador, several reports had been made regarding clayey and silty slope failures after raining periods, leaving behind high-cost damages and even human casualties [4, 5, 6]. For that reason, researchers had investigated the behavior of less permeable slopes under unsaturated conditions and how their strength is compromised by water infiltration [3, 4].

Pedone et al [3] modeled a uniform clay slope of the Southern Apennines, with its mechanical and index properties measured from undrained triaxial tests [7]. The results of this research revealed a reduction of the safety factor as a consequence of weight increase in raining periods. The destabilizing forces increased as the weight of slides rose. On the other hand, slices lost weight for evaporation periods, increasing the safety factor. Ng and Shi [1] modeled a clayey sand slope under drought and rain periods, with their mechanical properties measured in triaxial tests results and considering undrained mechanical behavior. Results showed that the safety factor varies rapidly during drought periods compared to infiltration periods, concluding that short drought periods compensated for the loss of resistance during wet seasons. Finally, Alonso et al [8] conducted similar research to Ng and Shi [1], and Pedone et al [3], but the computed values of SF were lower compared to the other researchers.

This paper evaluates the feasibility of the implementations of rheometer results to evaluate the time evolution of SF. This research explores a comprehensive study of the evolution of SF under changing environmental conditions. The rheometer allows computing the yielding function parameters and the modulus of the materials for different water contents. The research is dived into three stages. First, the mechanical properties are measured in a rheometer test. Second, the results of the remoter are implemented in a finite element software for pore water pressure computations and a limit equilibrium software for slope stability analysis (SEEP/W and SLOPE/W). Finally, the results are compared with those obtained by other authors [1, 3, 8].

2. Materials

This research used two types of soil materials obtained from the literature. Their response to deviator stresses is driven by cohesion, but also by their state of saturation. Matric Suction theory developed by Fredlund and Xing [9] was used in the description of the materials. It is important to state that a value of 1 million kPa is taken as the maximum value of matric suction that the modeled soils can reach, according to the literature [9]. Also, Perera et al [10] proposed a set of equations to

plot the characteristic curve based on grain-size distribution and index properties, which were used to obtain the parameters that serve as input values in SEEP/W [11]. The soil conductivity *k* behavior under unsaturated conditions is calculated following Eq 1 [10]:

$$k = \frac{\int_{\ln(\psi)}^{b} \frac{\theta_{e^y} - \theta_{\psi}}{e^y} \theta'_{e^y}\, dy}{\int_{\ln(\psi_{aev})}^{b} \frac{\theta_{e^y} - \theta_{sat}}{e^y} \theta'_{e^y}\, dy} \quad (1)$$

Rheometer tests results [12] were used to compute the Stress-Strain curves at different suction of a high plasticity clay. The clayey soil has a plasticity index of 50, a mass of particles smaller than 75 μm of 100%, a dry weight (γ) of 13.142 $kN.m^{-3}$ and a saturated volumetric water content w_s of 0.4835 $m^3.m^{-3}$ [12]. Tests results of the failure envelope in the suction-shear stress plane are presented in Fig 1a. A climatic chamber was used to measure the evaporation flux in the clay sample, which resulted in 3E-07 $m.s^{-1}$ [12]. The value for the internal friction angle for the high plasticity clay is taken as 0° [13] for it to behave in an undrained state of stress. The hydraulic conductivity of the clay was 1E-08 $m.s^{-1}$ [12].

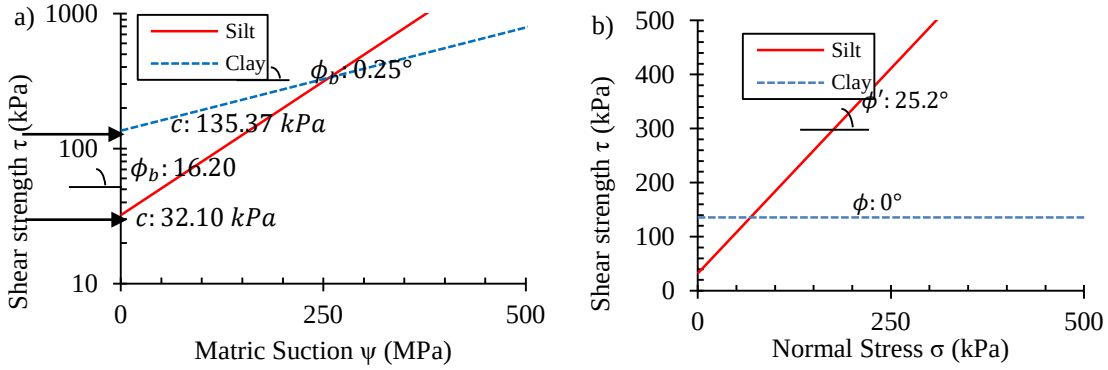

Fig.1: Strength parameters for the soil used in the stability model: a) Strength parameters of clay and silt, describing shear strength as a function of matric suction. b) Strength parameters of clay and silt, describing shear strength as a function of normal stress.

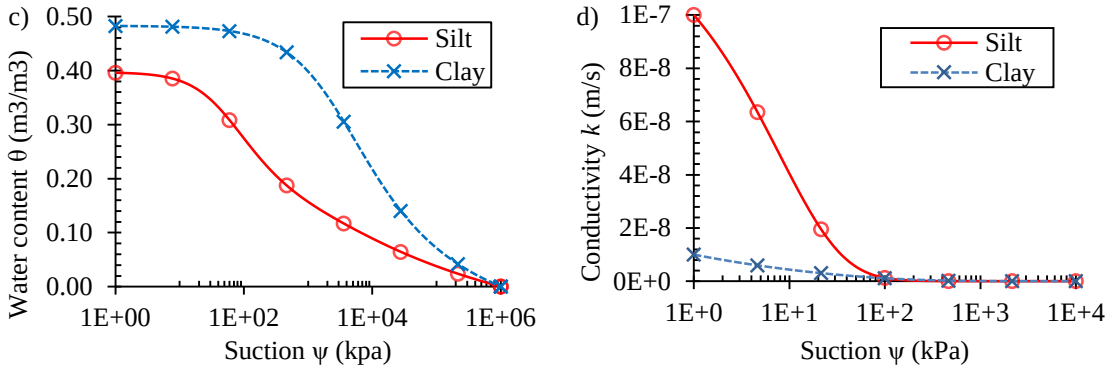

Fig 2: Soil behavior under unsaturated conditions: a) Soil-water characteristic curve built with Perera's parameters, that relates the water content in clay and silt with the experimented water suction. b) Conductivity in the model's clay and silt soil as a function of matric suction, representing Eq 1.

García-Navarro's results [14] were used to obtain the mechanical parameters of silty-sand soil. The results revealed that 64% of the soil mass was finer than 75 μm. Other important paramters of the material are summarized as follows: plastic index of 10, γ of 15.50 $kN.m^{-3}$ and w_{sat} of 0.3969 $m^3.m^{-3}$. ϕ_b was set to have a value of 16.2°, taken from the literature [13, 12].

3. Methods

Geometry of Model

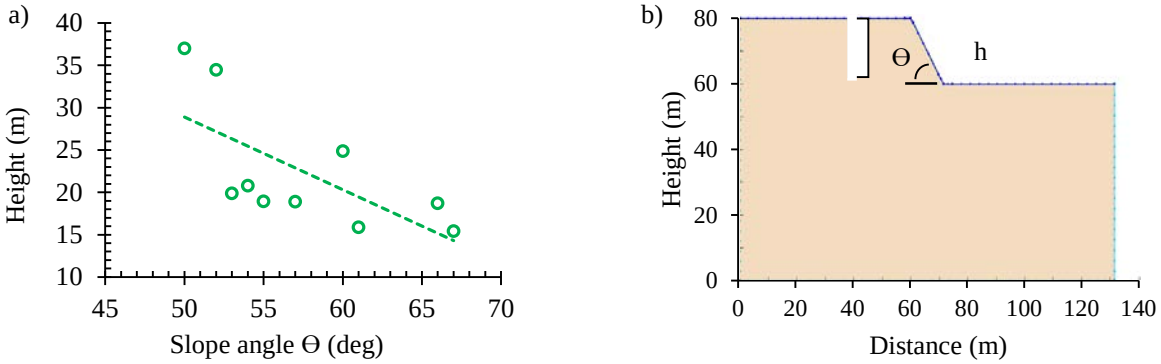

Fig.3: a) Scattered plot and best fit linear function for the characterized slopes [15]. b) Geometry of the model develop din GeoStudio, obeying the correlation in Eq 2.

The proposed slope's geometry was obtained from a study of the Avenue Simón Bolívar in Quito, Ecuador [15]. In this study, the experimental data were adjusted using linear regression. Eq 2 is the linear regression of this study, where it gives a relationship between the height of the slope (h) and the sloped angle (Θ).

$$h = 71.826 - 0.8585\Theta \quad (2)$$

The modeled geometry is based on the mentioned equation. Consequently, for a typical height of 20 m, the angle can be approximated to 60°. The geometry of the modeled slope is presented in Fig 3b.

Seep and Slope Modeling

The seepage analysis started with a fully saturated soil deposit, the de simulation was divided into two parts. First, the model was subjected to evaporation with a water flux of -3E-07 m/s. The evaporation simulation stopped once water suction of 1E6 kPa was reached. Then the second part started. In this part, the boundary condition of evaporation was changed to infiltration. The infiltration was set up close to the saturated hydraulic conductivity. The two materials described in the previous sections were used on this modeling configuration This research computes the slope stability through a limit equilibrium analysis at different times of the seepage analysis. Bishop´s limit equilibrium theory was used because it considers the variation in pore water pressure [16].

4. Results

Fig 4a to 4d show the contour lines of PWP and a cross mark 2.5m under the crown's surface. The PWP increases 50 kPa at that depth in the clay slope (after 1 year of rain), and 35 kPa in the silt slope (after 140 days). Alonso's model presented a faster increase in PWP, 75 kPa in 60 days [8]. Alonso's results differ from this research. This is explained by the greater permeability of the soil in the previous research.

A more significant variation in the PWP is observed in the drought period than in the raining simulation. This suggests that water will infiltrate significantly slower than evaporate under the studied water conditions. This fact is evidenced at the end of the rain simulation where the water table has not recovered its original position. The waterbed level stayed unaltered at the toe and lowered near the crown. The water conductivity in the slope is increased as saturation does. Therefore at the crown of the slope where the water table is lower than in the toe, the soil water conductivity will the lowest.

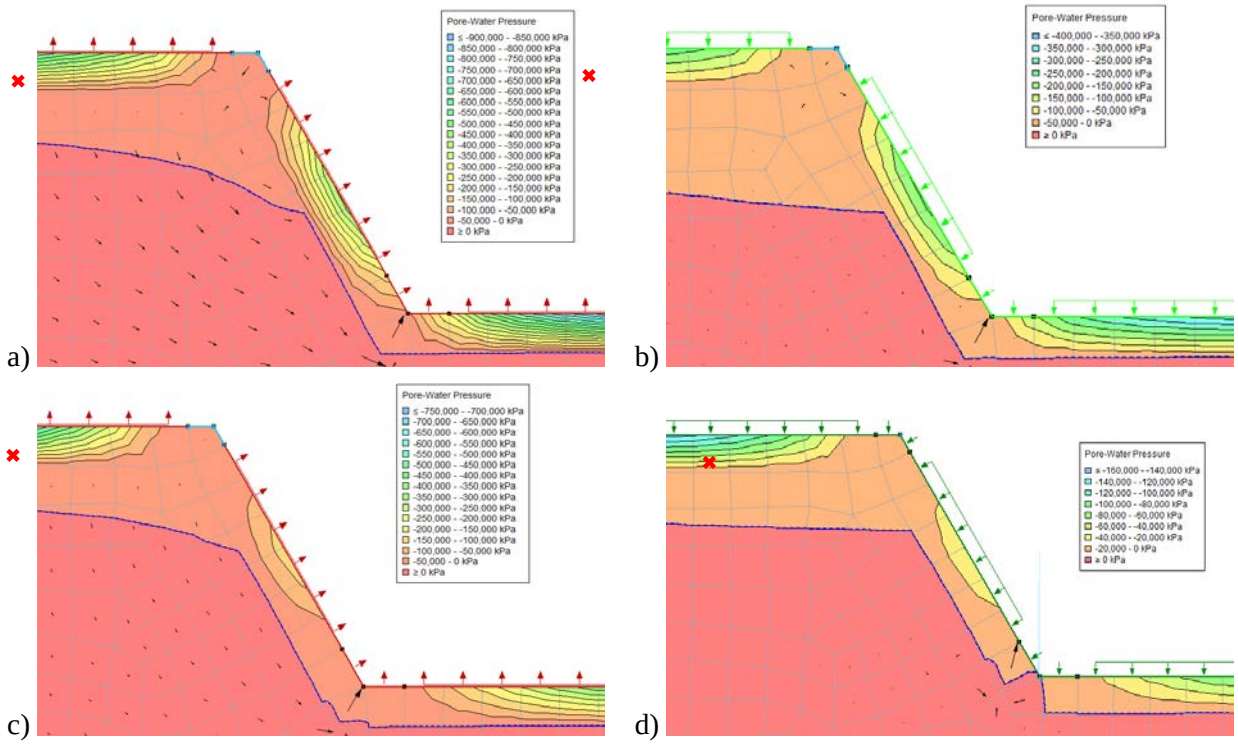

Fig 4: Contour lines of PWP in a) the clay slope at the end of the drought period, b) the clay slope at the end of the rain period, c) the silt slope at the end of the drought period, d) the silt slope at the end of the rain period.

Regarding the behavior of the SF through time, it increases during drought faster than it decreases with rain. During a drought in the clay slope, SF takes 41 days to increase by 1.98 and a year to decrease by 0.86. For the silt slope, SF increases 0.99 in 34 days and decreases 0.59 after 140 days. The behavior of the SF is similar to that presented by Ng and Shi [1], where drought periods compensate for the reductions of SF during extended periods of rain.

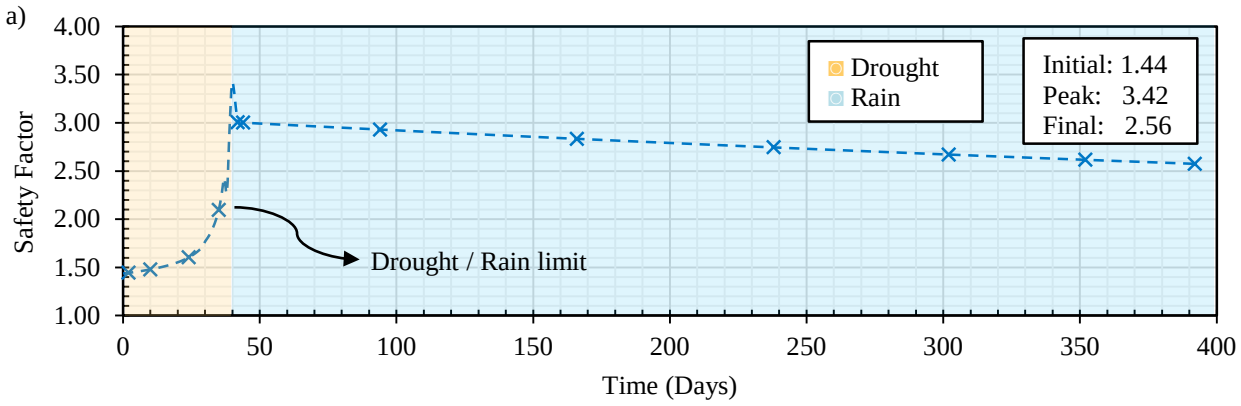

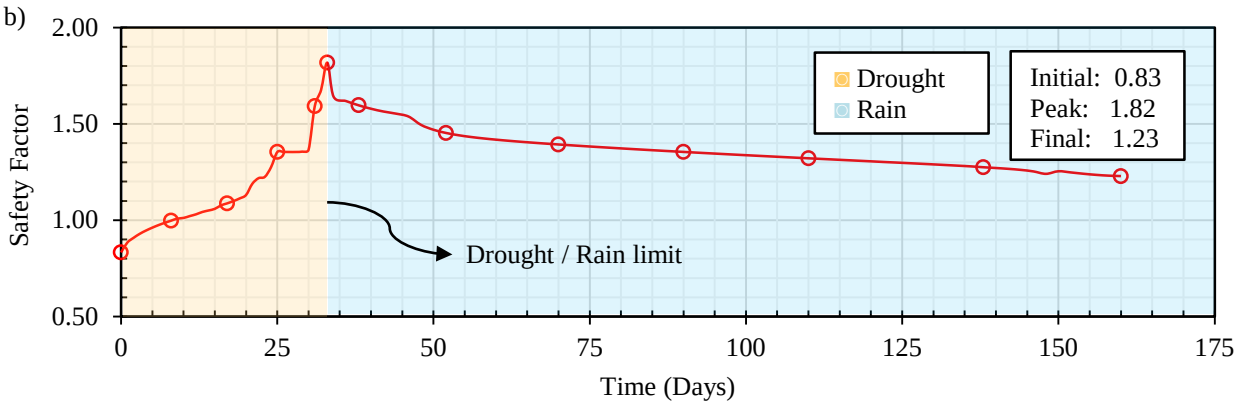

Fig 5: a) Evolution of the Safety Factor during drought and infiltration periods in the clay slope model. b) Evolution of the Safety Factor during drought and infiltration periods in the silt slope model.

Different stages of the transient analysis can be compared with the results in Fig 5a and Fig 5b. SF for the silt slope at a completely saturated state (initial state) has a value below 1.0, presenting instability until a week of drought has taken place. On the other hand, the strength parameters of the clay slope allowed computing an initial SF of 1.67. This suggests that silt slopes are more susceptible to losing their strength when saturation increase. A significant variation in the first days of rain is seen in both models, lowering SF by 12.28% in the clay slope and 12.08% in the silt slope. This suggests that a rain event after a long drought period has to be considered the maximum SF for design purposes.

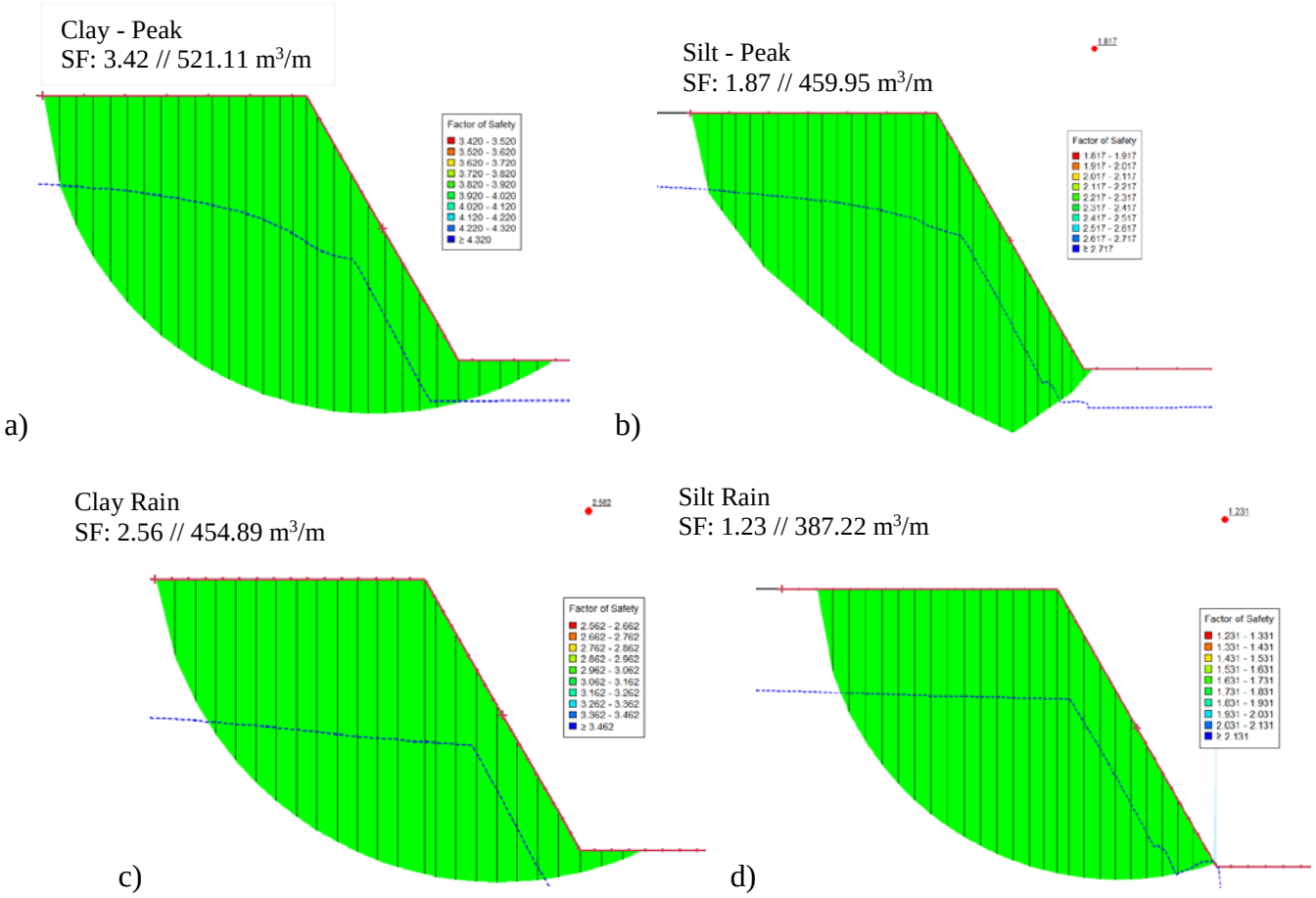

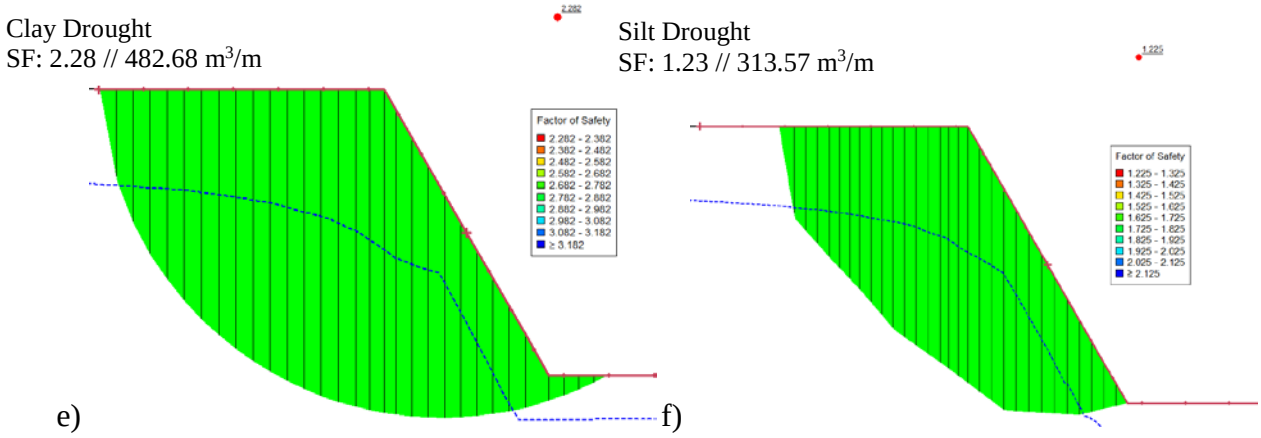

Fig 6: Critical slip surface at a) peak SF for the clay slope, b) peak SF for the silt slope. Critical slip surface at c) last valid SF for the clay slope, d) last valid SF for the silt slope. Drought-associated critical slip surface for e) the clay slope, with SF equal to Fig 5c, f) the silt slope, with SF equal to Fig 5d.

The mobilized mass of soil was measured and reported in Fig 6a to 6d. The mobilized mass of soil within the failure slope is greater at the end of the dought simulation than at the end raining. At the end of the rain period, the mobilized mass decreases by 12.71% in the clay slope and 15.81% in the silt slope when compared to its dry state. This behavior is opposite the SF, and a more significant mass is needed to induce failure in a dry slope due to the increased soil strength. When analyzing the same value of SF in the dought and rain simulation for the same material, the carried mass associated with the SF is higher in the drought simulation for clay slopes. For example, the mobilized mass for an SF close to 2.28 in the clay slope is 454 m3/m for the rain simulation whereas for drought is 482 m3/m. The effect in the silt slope was the opposite, the mobilized mass for the same SF was 387 for raining and 313.57 m3/m.

The mobilized mass is higher at end of the drought period, a bigger mass is needed to induce failure when the soil has its highest strength. In the drought simulation soil achieved the highest value of PWP on the surface of the slope; this lead to the failure surface to deeper depths.

5. Conclusions

The main objective was to evaluate the feasibility of rheometer tests results to describe the evolution of the SF throughout the drought and rainy seasons. Strength parameters were taken from rheometer tests for the clay slope model, while external data was taken for the silt slope model. SEEP/W and SLOPE/W software were used to analyze the evolution of pore water pressure and the safety factor. The simulation was interrupted when the slope reached a surface suction of 1 million kPa. An evaporation boundary condition of 3E-07 m/s was applied on two models. The first model was constructed using the properties of the clay soil, while the second used the properties of silty sand. The maximin suction was achieved in 41 days for the clay slope, while for the silty slope in 34 days. Then, an infiltration close to the saturated water conductivity was applied as a boundary condition in both models. The results revealed a faster evolution of the factor of safety in the evaporation simulation than compared to infiltration.

SF increased rapidly during drought periods and decreased gently during rain. The model also matched sudden decrements of the SF in rain events after extended periods of drought. The decrement in the SF and rise in the PWP were slower compared to the results of infiltration. The model described peaks for both slopes after the maximum matric suction was achieved. The mobilized mass associated with the critical slip surfaces was also compared. The mobilized mass with the same SF during drought and rain periods for the silt slope shows that more mass of soil is needed in rain seasons to cause the slope failure. It is concluded that slope stability models that work with strength parameters taken from rheometer tests are appliable.

6. References

[1] C. Ng and Q. Shi, *Influence of rainfall intensity and duration on slope stability in unsaturated soils,* vol. 31, Hong Kong: Quarterly Journal of Engineering Geology, 1998, pp. 105-113.

[2] H. Rahardjo, E. C. Leong, M. Deutscher, J. Gasmo and S. K. Tang, *Rainfall-induced slope failures,* Singapore: NTU-PWD Geotechnical Research Centre, 2000.

[3] G. Pedone, G. Ruggieri and R. Trizzino, *A contribution to the use of numerical modelling for the characterisation of climatic variables aimed at identifying instability thresholds in clay slopes,* vol. 8, Géotechnique Letters, 2018, pp. 231-239.

[4] P. Montalvo, S. Sánchez, J. D. López and A. Estévez, *LOS TALUDES DE LA VÍA ALÓAG-SANTO DOMINGO. EMPLEO DE DRONES PARA LA CARACTERIZACIÓN DE INESTABILIDADES,* Santander: IX Simposio Nacional sobre Taludes y Laderas Inestables, 2017.

[5] J. L. Rosales, "Tres niños mueren a causa de un deslave en Carchi," 19 november 2021. [Online]. Available: https://www.elcomercio.com/actualidad/ecuador/ninos-mueren-deslave-carchi-lluvias.html.

[6] W. Wilcke, H. Valladarez, R. Stoyan, S. Yasin, C. Valarezo and W. Zech, *Soil properties on a chronosequence of landslides in montane rain forest, Ecuador,* vol. 53, Bayreuth: CATENA, 2003, pp. 79-95.

[7] F. Cotecchia, C. Vitone, F. Santaloia, G. Pedone and O. Bottiglieri, *Slope instability processes in intensely fissured clays: case histories in the Southern Apennines,* vol. 12, Bari: Landslides, 2015, pp. 877-893.

[8] E. Alonso, A. Gens and C. Delahaye, *Influence of rainfall on the deformation and stability of a slope in overconsolidated clays: a case study,* vol. 11, Hydrogeology Journal, 2003, pp. 174-192.

[9] D. Fredlund and A. Xing, *Equations for the soil-water characteristic curve,* vol. 31, Saskatoon: Can. Geotech, 1994, pp. 521-532.

[10] Y. Y. Perera, C. E. Zapata, W. N. Houston and S. L. Houston, *Prediction of the soil-water characteristic curve based on grain-size-distribution and index properties,* Advances in Pavement, 2005, pp. 1-12.

[11] GEO-SLOPE International, Ltd., *Seepage Modeling with SEPP/W,* Calgary: GEO-SLOPE International, Ltd., 2012.

[12] J. Villacreses, J. Granados, B. Caicedo, P. Torres and F. Yépez, *Seismic and hydromechanical performance of rammed earth walls under changing environmental conditions,* vol. 300, Construction and Building Materials, 2021.

[13] B. Das, *Fundamentos de Ingeniería Geotécnica,* México D.F.: Thomson Learning, 2001.

[14] E. García-Navarro, M. Camacho, J. Morales and F. Alonso, *Análisis de estabilidad en taludes arenosos: deslizamientos en "Los Cabezos" de Huelva,* vol. 24, Revista de la Sociedad Geológica de España, 2011, pp. 101-115.

[15] E. Montatixe and D. Chango, *Análisis de estabilidad de taludes en un tramo de las avenidas Simón Bolívar y Gonzalo Pérez Bustamante, Distrito Metropolitano de Quito,* Quito: Faciltad de Ingeniería en Geología y Petróleos, EPN, 2018.

[16] GEO-SLOPE International, Ltd., *Stability Modeling with SLOPE/W,* Calgary: GEO-SLOPE International, Ltd., 2012.

[17] N. Lu and W. Likos, *Unsaturated Soil Mechanics,* Hoboken: John Wiley & Sons, 2004.